Dynamics of a shallow fluidized bed

Lev S. Tsimring,[1] Ramakrishna Ramaswamy,[2] and Philip Sherman[1]
[1]*Institute for Nonlinear Science, University of California, San Diego, La Jolla, California 92093-0402*
[2]*School of Physical Sciences, Jawaharlal Nehru University, New Delhi 110 067, India*
(Received 24 May 1999)

The results of the experimental study of the dynamics of a shallow fluidized bed are reported. The behavior of granular material is controlled by the interplay of two factors—levitation due to the upward airflow, and sliding back due to gravity. Near the threshold of instability, the system shows critical behavior with remarkably long transient dynamics. The experimental observations are compared with a simple cellular automata model. [S1063-651X(99)03812-X]

PACS number(s): 45.05.+x, 47.54.+r, 47.35.+i

I. INTRODUCTION

Fluidized beds are widely used in industry for mixing solid particles with gases or liquids [1]. In most industrial applications, a fluidized bed consists of a vertically oriented column filled with granular material, and a fluid (gas or liquid) is pumped upward through a distributor at the bottom of the bed. When the the drag force of flowing fluid exceeds gravity, particles are lifted and fluidization occurs. A uniform fluidization which is the most desirable regime of operation of industrial fluidized beds, is prone to instabilities. As the fluid flow increases, bubbles of clear fluid are formed at the bottom of the bed and these bubbles travel to the surface. The study of mechanisms of fluid bed instabilities and the classification of ensuing regimes (slugging, bubbling, etc.) has been an active area of research among engineers. Recently, there has been an increasing interest to study of complex fluidized bed dynamics among physicists. The research has been mainly focused on deep fluidized beds whose vertical dimension is larger than the characteristic size of the bubbles and (typically) the horizontal dimensions of the chamber. In a number of papers pressure fluctuations on a side wall of the fluidized bed has been measured and related to the processes inside the bed. In particular, large quasiperiodic oscillations of the pressure are produced by slugging. A sequence of bifurcations leading to possibly chaotic fluidized state has been observed in Refs. [2,3], however, some other authors dispute the occurrence of low-dimensional chaos in fluidized beds (see Refs. [4,5]). Much attention has been paid to the detailed theoretical and experimental studies of bubble formation and propagation through a column of granular material [6,7]. Recent advances in instrumentation allowed to carry out accurate measurements of the particle motions inside the bed. Menon and Durian [8] used diffusion-wave optical spectroscopy and showed that in the regime of uniform fluidization, there is no persistent particle motion particles. It was emphasized that only bubbling motion is the source of all particle dynamics in the bed.

Much less attention has been devoted to the study of shallow fluidized beds (perhaps due to their lesser technological importance rather than lack of fundamental physical interest) [9]. When the height of the bed is much smaller than its horizontal size and characteristic bubble size for an equivalent deep bed, no bubble formation can be expected. A natural question arises on what sequence of regimes leads to a developed turbulent fluidized state in that system. Because of the large aspect ratio, the dynamics is effectively two dimensional, which allows one to gain much information by simply observing the bed from above [10].

A goal of the present work is to study experimentally the transition from a static to a fluidized state in a shallow bed as the air flow through the bed is increased. We employ image processing in order to detect the particle motion. We show that below certain threshold value of the the air flow, the bed exhibit transient dynamics in a form of localized regions of activity which gradually disappear and eventually the bed comes to a completely motionless metastable state. This state is similar to the one described in Ref. [8] as a motionless uniformly fluidized state. Slightly above the critical air flow, the localized active regions do not disappear but move slowly across the bed in a seemingly random fashion. At large air flow the active regions merge and the whole bed becomes active. The surface of the bed is similar to that of a boiling fluid. It develops a rather irregular oscillating cellular pattern. These oscillating cells apparently have an origin related to that of bubbles in deep fluidized beds, however, the detailed study of this regime goes beyond the scope of the present publication. In order to elucidate the mechanism of transition from the static to a dynamic state, we proposed a cellular automaton (CA) model which simulates the fluidization and relaxation processes in a shallow fluidized bed. This model exhibits a similar critical behavior as the control parameter is varied.

II. EXPERIMENT

The experiment was performed in a Plexiglas cell with a rectangular cross section of dimension 2.5×3 cm^2. We used nonspherical bronze particles of characteristic size 0.2 mm, and the layer thickness was about 10 particles. The bottom plate was made of a sintered steel with an average pore size 5 μm. Dry air was pumped through the layer, and the pressure drop Δp across the layer and the porous plate served as a control parameter. The top-view images of the surface of the granular layer were taken using a standard CCD camera at a frame rate 30 fps and digitized with a frame grabber Matrox Meteor-II. The typical resolution of the frames was 300×400 pixels covering a region of approximately 5 cm^2.

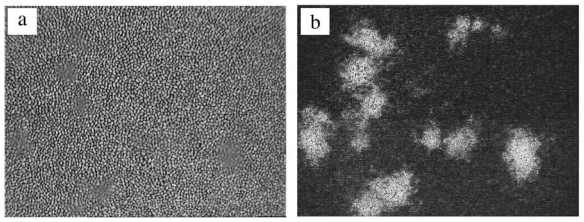

FIG. 1. (a) Photograph of the surface of the thin granular layer obtained with exposition 0.8 sec. (b) Corresponding differential surface image.

Active regions with agile particles are clearly visible by the naked eye, but they do not show well on snapshots. If taken with long exposure, they appear as smeared spots against the sharp background of grains [see Fig. 1(a)]. In order to detect active areas we computed ''differential'' images by subtracting two consecutive images from each other. Figure 1(b) shows the differential image corresponding to Fig. 1(a). Bright spots in the differential image correspond to active areas where grain were moving, whereas in the black background they were motionless.

The total instantaneous brightness of the differential image characterizes the space-averaged activity of the layer. We measured this brightness B as a function of time for different values of the control parameter (air pressure drop) Δp [11]. The typical results are shown in Fig. 2, where every time series corresponds to several sequential experimental runs initiated by slight tapping of the bed (the beginning of each run is marked by the sharp rise of brightness).

For Δp below a certain threshold value Δp_c, the activity eventually ceases, and the granular layer becomes frozen despite the persistent air flow. In each of the multiple runs, we measured the characteristic relaxation time. Figure 3 shows the characteristic relaxation time as a function of the pressure drop, averaged over multiple runs performed at the same values of parameters. The characteristic time of decay increases with Δp, see Fig. 3(a). Error bars in this figure indicate the minimum and maximum values of T over 10 runs. Near the critical value of the pressure drop $\Delta p_c \approx 33.5$ kPa, the characteristic relaxation time seems to diverge. At Δp slightly below Δp_c, the fluctuating activity sometimes persists for a long time and then it rapidly decays to zero. The time of this transition varies widely from run to run [see Fig. 2(b)], hence large error bars near the critical point in Fig. 3(a). Visually, long relaxation times occur whenever a single large active spot is formed [see Fig. 4(a)]. If, however, activity is spread among many smaller spots [Fig. 4(b)], it decays more rapidly. It seems that breakdowns of activity in large spots are caused by occasional large fluctuations and without them the activity would be persistent. It indicates that the fluidization transition in this geometry is probably first order. For yet larger values of $\Delta p > \Delta p_c$ active regions never disappear, however, large fluctuations in the amount of fluidization activity are observed. Figure 3(b) shows the asymptotic value of space-time average brightness B as a function of Δp for $\Delta p > \Delta p_c$. Here error bars indicate maximum and minimum values of B over 10-min intervals of measurements. One can see that brightness grows with Δp. The range of brightness fluctuations is large at small $10.0 < \Delta p < 10.3$ due to the apparent bistability of the fluidized

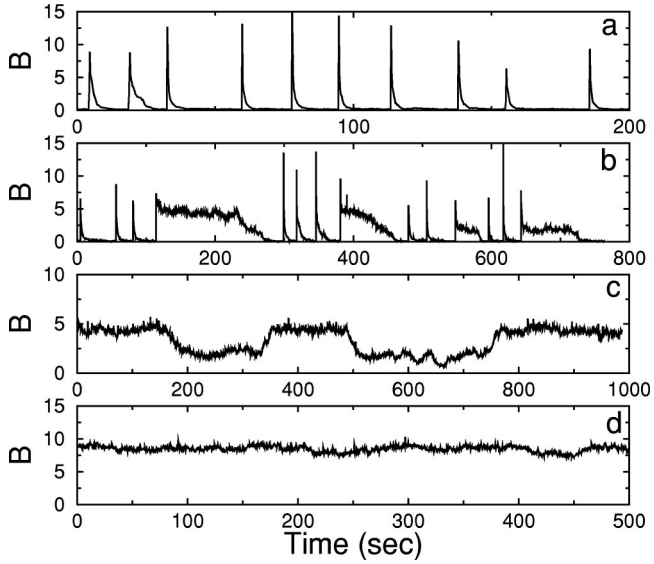

FIG. 2. Temporal evolution of the spatially averaged brightness of differential images for various values of the pressure drop $\Delta p = 31.3$ kPa (a), 32.9 kPa (b), 34.1 kPa (c), and 35.6 kPa (d). Sharp rises of brightness correspond to the moments when the bed was tapped to create a new initial particle configurations.

state. Indeed, these fluctuations have a form of rapid switching between two metastable levels of activity [see Fig. 2(c)]. At large values of Δp these jumps disappear [Fig. 2(d)]. The activity involves whole layer, and the granular material dynamics resembles a boiling liquid. Study of this latter regime goes beyond the scope of this paper and will be presented in a separate publication.

III. CELLULAR AUTOMATON MODEL

In shallow fluidized beds, the dynamics is controlled by the interplay of two mechanisms: (i) levitation due to the upward fluid flow and (ii) relaxation due to the gravitational downflow of particles along the slopes, as in sandpiles. These dynamics can be simulated by the following simple cellular automaton model which is patterned on the lattice sandpile models that have been extensively studied recently [12,13].

We consider a one-dimensional (1D) lattice with N sites on which N_p particles are initially distributed at random. The integer dynamical variable $h_i(n)$ is the number of particles at site i at time n, which corresponds to the local layer height in the experimental system.

The dynamics of this 1D non-Abelian lattice sandpile [13] proceeds in two alternating half steps, fluidization and relaxation. In the fluidization half step, if the local height $h_i(n)$ is smaller than a fluidization threshold H_f, it is reduced by one and the height of one of its two nearest neighbors $h_{i\pm1}$ (picked at random) is increased by 1. In the relaxation step, if the local slope $h_i - h_{i\pm1}$ is greater than a relaxation threshold H_r, one particle moves from site i to site $i\pm1$ along the local slope. (If site i is a local maximum with supercritical slopes both towards $i+1$ and $i-1$, the direction of the slide is picked at random.) We update all sites synchronously at both the fluidization and relaxation steps. Note that the dynamics conserves the total number of particles N_p, and the

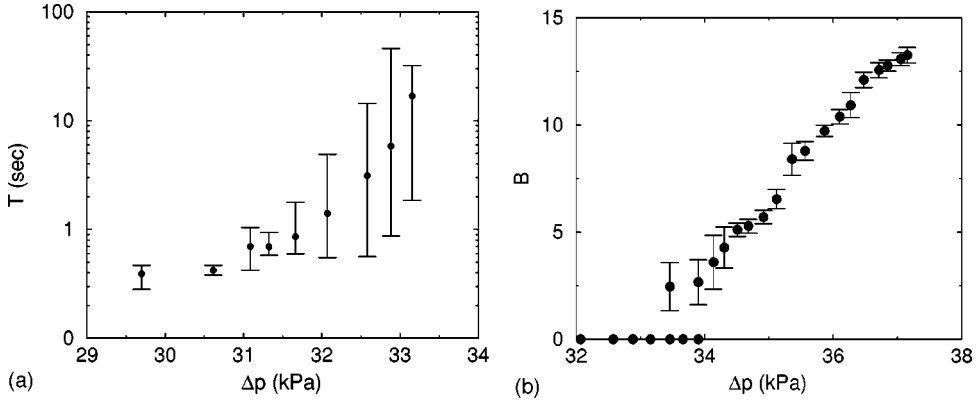

FIG. 3. Characteristic relaxation time T (a) and long-term averaged differential image brightness B (b) vs pressure drop Δp. Circles indicate average values, and error bars indicate the range of relaxation times over 10 runs, and the range of brightness over 10 min observations, for each value of Δp.

average layer height $\rho = N_p/N$ serves as a control parameter of the model.

Several examples of the model evolution are shown in Fig. 5, where the local height of the layer is gray coded and time progresses downwards. In these simulations, and throughout this section, we use the values $H_f = 3$ and $H_r = 1$, and apply periodic boundary conditions. Active sites are defined as those where there is a fluidization instability, namely, those for which $h_i(n) \neq h_i(n-1)$. These migrate along the lattice, and interact both with themselves as well as with ''hills,'' namely, sites with $h_i > H_f$. Clearly, if $\rho < H_f$, the dynamics of the model never terminates, as there always are sites with $h_i < H_f$. If $\rho > H_f$, the system ultimately reaches a stationary state where $h_i > H_f$ for all i.

Figure 6 shows the number of active sites as a function of time for several values of ρ. As can be expected, this decreases with time, eventually going to zero. As $\rho \to H_f$, though, this relaxation process may take very long times. In this limit, at the late phase of the relaxation there remain only few well separated active sites. Most of the lattice by that time is flattened out at the critical height H_f, and only few hills remain [see Fig. 5(b)]. It is easy to see that a solitary active site with $h_i = H_f - 1$ surrounded by sites with $h_j = H_f$ $(j \neq i)$ performs a classic unbiased random walk [14,15]. Indeed, suppose that after a fluidization half step, a particle moves from site i to $i-1$. Then, we have $h_i^f = H_h - 2$, $h_{i-1}^f = H_f + 1$. Since the relaxation threshold is $H_r = 1$, both slopes of the site i are supercritical, and two particles will jump to it from $i+1$ and $i-1$ at the next relaxation half step. After that, site $i+1$ will become active instead of site i and the process repeats. (With different values for the thresholds H_f and H_r, this argument needs to be slightly modified.) Active sites perform a random walk until they collide with immobile hills and are annihilated.

The asymptotic dynamics of the above CA model is equivalent to the fluctuation-dominated kinetics of the irreversible bimolecular reaction $A + B \to 0$ [16]. In this reaction, particles of two different species A and B perform random walks in one dimension until they meet and instantly annihilate. For equal initial concentrations of both species $[C_A(0) = C_B(0)]$ and exactly uniform initial spatial distribution of particles, the mean-field theory predicts fast $1/kt$ decay of the concentrations of both species if they have equal concentrations, or even faster exponential $[\propto \exp(-kt)]$ decay of one species if the initial concentrations are different (k is the rate constant related to the mobility of particles and their effective cross section). However, if the initial spatial distribution of particles is random, as a result of many annihilation events relative fluctuations of concentrations amplify and lead to formation of alternating A-rich and B-rich domains. Now for a particle A to annihilate with its B counter-

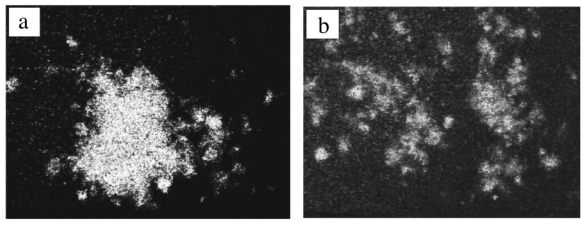

FIG. 4. Spatial distributions of active particles corresponding to long (a) and short (b) relaxation times for $\Delta p = 33.0$ kPa.

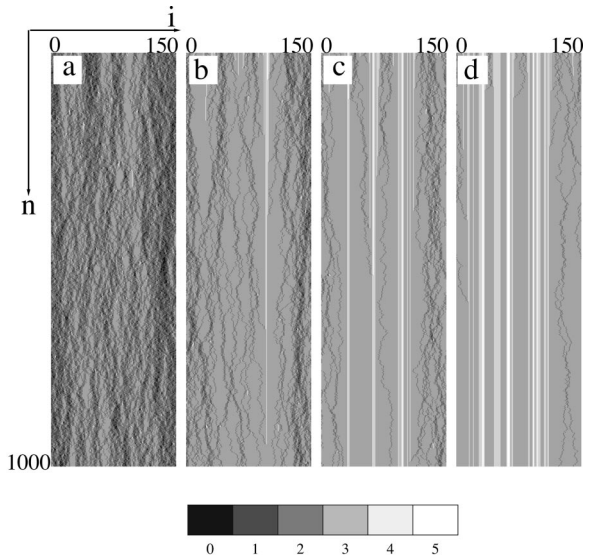

FIG. 5. Space-time diagrams of the cellular automata evolution at several values of ρ for $N = 150$, $H_f = 3$, $H_r = 1$. (a) $\rho = 2.0$, $\rho = 2.7$, (b) $\rho = 3.0$, (c) $\rho = 3.3$; 1000 iterations, time goes from top to bottom; shades of gray correspond to the local height according to the color map above

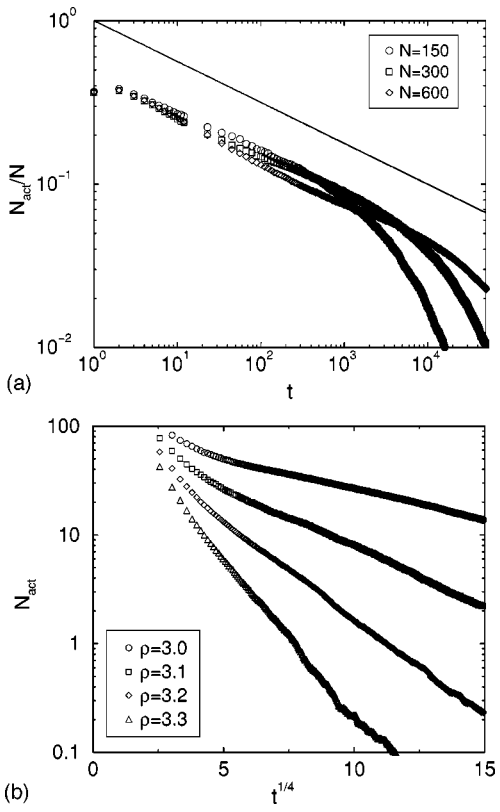

FIG. 6. A number of active sites in the CA model with $H_f=3$, $H_r=1$ as a function of time: (a) for different system sizes N at the critical value of $\rho=3.0$, (b) for different values of ρ at $N=600$. The solid line in (a) indicates $-1/4$ slope

part, it has to travel across an A-rich domain to its boundary. Therefore, the decay of concentrations becomes much slower, $C_{A,B}\propto t^{-d/4}$ [15] where d is the spatial dimension of the system.

This agrees both qualitatively and quantitatively with the results of Monte Carlo simulations of the CA model. Domains can be observed in Figs. 5(c) and 5(d), where the barriers to relaxation can be clearly seen. The power-law decay of the number of active sites at the critical value of $\rho=\rho_c$ is also confirmed by simulations: the straight line in Fig. 6(a) corresponds to a slope $-1/4$. Deviations from power-law behavior at large times is caused by finite-size effects; indeed, when the average distance between active sites becomes of the order of the system size, the annihilation proceeds at an exponential rate, inversely proportional to N.

The case of $\rho\neq\rho_c$ corresponds to annihilation of particles with unequal initial concentrations. In this case, at the late stage of the evolution, one type of particle (A, say) survives, with the limiting concentration $C_A(\infty)=C_A(0)-C_B(0)$, while that of the other type decays exponentially,

$$C_B(t)\propto\exp\{[C_A(0)^{1/2}-C_B(0)^{1/2}]t^{d/4}\} \quad (1)$$

at a rate which depends on the concentration difference. This result also agrees well with Monte Carlo simulations of the CA model at $\rho>H_f$ [see Fig. 6(b)].

The precision of the experimental data does not, at present, allow us to verify these theoretical predictions in a quantitative manner. More systematic measurements in a bigger system are needed. Furthermore, the experiment is carried out in a two-dimensional cell, while numerical simulations are for a one-dimensional lattice, although the model can be generalized to higher dimensions.

IV. CONCLUSIONS

To conclude, in this paper we studied the transition to a fluidized state in a shallow granular layer. Experiments with air-driven shallow fluidized bed showed that fluidization begins in localized active regions. Below a certain critical magnitude of the air flow, the activity eventually ceases, sometimes after a long transient. Above a fluidization threshold, the activity is persistent. Near the threshold the magnitude of activity remains nearly constant for a long time (several minutes) before it rapidly disappears due to a particularly large fluctuation. This indicates the presence of a first order transition to the fluidized state. We proposed a simple cellular automata model describing fluidization in a shallow granular layer. The model involves two local mechanisms of grain dynamics: fluidization and relaxation. An interplay between these two mechanisms yields a transition to a fluidized state similar to that observed experimentally. The important difference is, however, that the transition in the model is continuous, while in the experiment there is an apparent hysteresis. We believe that the hysteretic behavior of the shallow fluidized bed is due to the long-range coupling between the sites which is missing in the current model. A study of the global dynamics of the shallow fluidized bed will be the subject of future work.

ACKNOWLEDGMENTS

This research was supported by the U.S. Department of Energy Grant Nos. DE-FG03-95ER14516 and DE-FG03-96ER14592. R.R. would like to thank the Institute for Nonlinear Science for hospitality.

[1] A.M. Squires, M. Kwauk, and A.A. Avidan, Science **230**, 1329 (1985).
[2] C.M. Van Den Bleek and J.C. Schouten, Chem. Eng. J. **53**, 75 (1993).
[3] C.S. Daw, W.F. Lawkins, D.J. Downing, and N.E. Clapp, Jr., Phys. Rev. A **41**, 1179 (1990).
[4] S.W. Tam and M.K. Devine, in *Measures of Complexity and Chaos,* edited by N.B. Abraham *et al.* (Plenum, New York, 1989).
[5] N. Letaief, C. Rosé, and G. Gouesbet, J. Phys. II **5**, 1883 (1995).
[6] G.K. Batchelor, J. Fluid Mech. **257**, 359 (1993).
[7] J.F. Davidson and D. Harrison, *Fluidized Particles* (Cambridge University Press, London, 1963).
[8] N. Menon and D. Durian, Phys. Rev. Lett. **79**, 3407 (1997).
[9] U. Schaflinger *et al.*, Int. J. Multiphase Flow **23**, 455 (1997).
[10] In this respect, the shallow fluidized bed is similar to another popular pattern-forming system, namely, Rayleigh-Benard

convection which is observed in a thin layer of fluid between two solid walls heated from below.

[11] For our thin granular layer, the pressure drop is mostly determined by the porous plate and, according to Darcy's law, is directly proportional to the air flow rate. We checked directly that removing the granular material led to changes in the pressure drop of the order of 5%.

[12] P. Bak, C. Tang, and K. Wiesenfeld, Phys. Rev. Lett. **59**, 381 (1987).

[13] D. Dhar, Physica A **263**, 4 (1999).

[14] W. Feller, *An Introduction to Probability Theory and Its Application* (New York, Wiley, 1968).

[15] D. Toussaint and F. Wilczek, J. Chem. Phys. **78**, 2642 (1983): K. Kang and S. Redner, Phys. Rev. A **32**, 435 (1985).